Ten Years of Experience With a Small Jet Engine as a Support for Education

O. Léonard
Professor
e-mail: o.leonard@ulg.ac.be

J. P. Thomas
FNRS Research Fellow
e-mail: jp.thomas@ulg.ac.be

S. Borguet
Research Engineer
e-mail: s.borguet@ulg.ac.be

Turbomachinery Group,
University of Liège,
Chemin des Chevreuils, 1
B-4000 Liège, Belgium

In 1997 the Turbomachinery Group of the University of Liège decided to acquire a small jet engine to illustrate the courses in propulsion and to provide the students with the opportunity to get some experience on data measurement, acquisition, and interpretation. Among others, the SR-30 engine from Turbine Technology Ltd. Chetek, WI was chosen. It consists of a single spool, single flow engine with a centrifugal compressor, a reversed combustion chamber, an axial turbine, and a fixed convergent nozzle. This engine was installed on a test bench allowing for manual control and providing fuel and oil to the engine. The original setup included measurements of intercomponent pressure and temperatures, exhaust gas temperature, and rotational speed. Since then both the engine and the test bench have been deeply modified. These modifications were led by a triple objective: the improvement and the enrichment of the measurement chain, the widening of the engine's operational domain, and, last but not the least, the wish to offer appealing hands-on projects to the students. All these modifications were performed at the University of Liège and were conducted by the students as part of their Master theses. Several performance models of the engine were developed to support data validation and engine condition diagnostic. This paper summarizes the developments conducted with and by the students, and presents the experience that was gained by using this engine as a support for education. [DOI: 10.1115/1.2967487]

Keywords: jet engine, test bench, hands-on projects, Master students

1 Introduction

The Department of Aerospace and Mechanical Engineering of the University of Liège, Belgium offers undergraduate and graduate programs leading to Bachelor, Master, and Ph.D. degrees in Aerospace, Mechanical, and Energetics Engineering. Air-breathing propulsion is one of the key issues of the Master in Aerospace engineering, whose objective is to train the students in advanced techniques of modeling, simulation, and measurements in the disciplines involved in aerospace: fluid mechanics, flight mechanics, solid mechanics, propulsion, and materials.

In 1997 the Turbomachinery Group of the University of Liège decided to acquire a small jet engine to illustrate the lessons in propulsion. The nature of the funding clearly oriented the project toward didactic activities more than research ones, although both are often coupled. The idea was to provide the students with the opportunity to get some experience on data measurement, acquisition, and interpretation.

The engine had to be not too big so that it can be operated in a university laboratory environment, without too drastic security measures, and not too small so that it offers enough didactic possibilities. Indeed there are quite a few jet engines for model aircrafts that are offered now at a reasonable price, but they are so small that it is unlikely that they can be equipped with a few sensors for intercomponent pressure and temperatures.

The SR-30 engine from Turbine Technology Ltd. was chosen among others. This was also the choice of other teams, such as Refs. [1–3]. The SR-30 is a single spool, single flow engine with a centrifugal compressor, a reversed combustion chamber, an axial turbine, and a fixed convergent nozzle (Fig. 1). This engine is installed on a test bench, which allows manual engine control and provides fuel, oil, and pressurized air for the starting procedure (Fig. 2).

Since 1997 both the engine and the test bench have been deeply modified. These modifications were led by a triple objective: the improvement and the enrichment of the measurement chain, the widening of the engine's operational domain, and, last but not the least, the wish to offer appealing hands-on projects to the students. The fittings and connections of the engine to the bench were completely changed and a load cell was added to measure the thrust. A variable area nozzle was mounted on the engine so as to modify the engine working line. Variable geometry inlet guide vanes were added ahead of the compressor wheel to modify the compressor characteristic. A servomotor was added to remotely operate the fuel valve and to control the engine using the acquisition system. Besides additional sensors were added such as a fuel flowmeter and an air flowmeter.

All these modifications were performed at the University of Liège and were conducted by the students as part of their Master theses. Several thermodynamical performance models of the engine were also developed to support data validation, new component design (inlet guide vane and nozzle), engine condition diagnostic, and engine control. This paper summarizes the developments conducted with and by the students, and presents the experience that was gained by using this engine as a support for education.

2 The Original Engine

The SR-30 engine from Turbine Technology Ltd. is 170 mm $\times 270$ mm. It is a single spool, single flow engine with a centrifugal compressor, a reversed combustion chamber, an axial turbine, and a fixed convergent nozzle. This engine has the ability to run on different fuels, such as diesel, but using kerosene makes it easier to start. The design operating point is defined as

Contributed by the International Gas Turbine Institute of ASME for publication in the Journal of Engineering for Gas Turbines and Power. Manuscript received April 1, 2008; final manuscript received April 8, 2008; published online October 10, 2008. Review conducted by Dilip R. Ballal. Paper presented at the ASME Turbo Expo 2008: Land, Sea and Air (GT2008), Berlin, Germany, June 9–13, 2008.

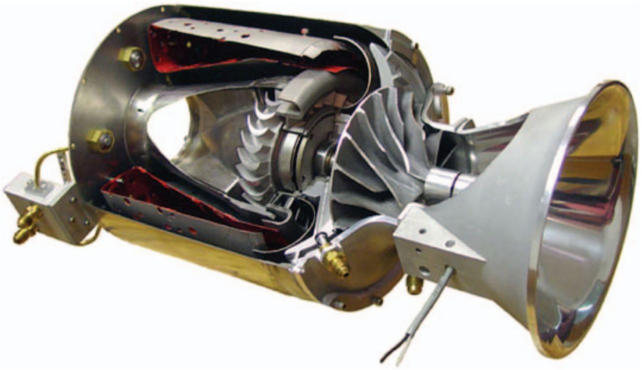

Fig. 1 Cutaway of the SR-30 engine

Thrust: 140 N	Fuel flow: 0.005 kg/s
EGT: 720°C	Airflow: 0.5 kg/s
Speed: 86,000 rpm	Compression ratio: 3.4

The engine is installed on a test bench, which allows manual engine control and provides fuel, oil, and pressurized air. In 1997 the original setup included measurements of some intercomponent pressure and temperatures, exhaust gas temperature (EGT), and rotational speed. The thrust was not directly measured but correlated with the pressure in the combustion chamber. Neither the airflow nor the fuel flow was available at that time. Since then significant modifications have been brought by the manufacturer [4]. The data acquisition is obtained with a National Instruments SCXI chassis and displayed with LABVIEW.

3 Hardware Modifications

During initial testing of the SR-30, it was found that some variables were mandatory in order to perform a complete energy balance on the jet engine: the thrust, the airflow, and the fuel flow. Also, it came out that it would be interesting to control the position of the engine equilibrium line. It was decided to build a variable area nozzle and to mount it downstream of the existing one, as a prolongation of the latter. Later it was also decided to build a variable geometry inlet guide vane to be mounted between the bell-mouth inlet and the compressor wheel, so as to be able to modify the compressor characteristic. Finally it was decided to explore the possibility of controlling the engine using the data acquisition system and a servomotor was added to remotely operate the fuel valve.

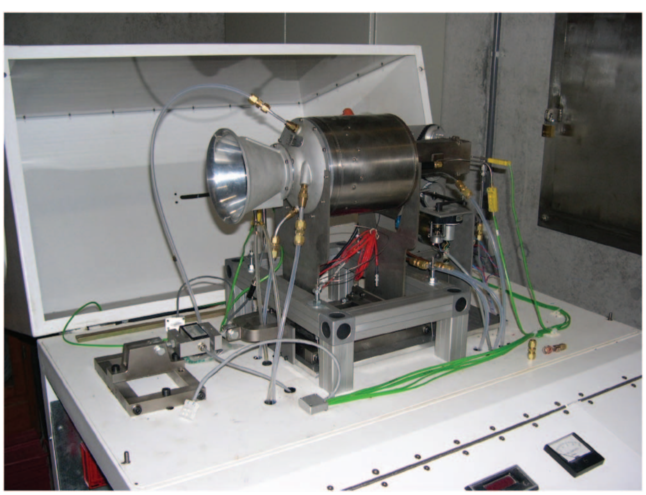

Fig. 2 SR-30 engine on its test bench

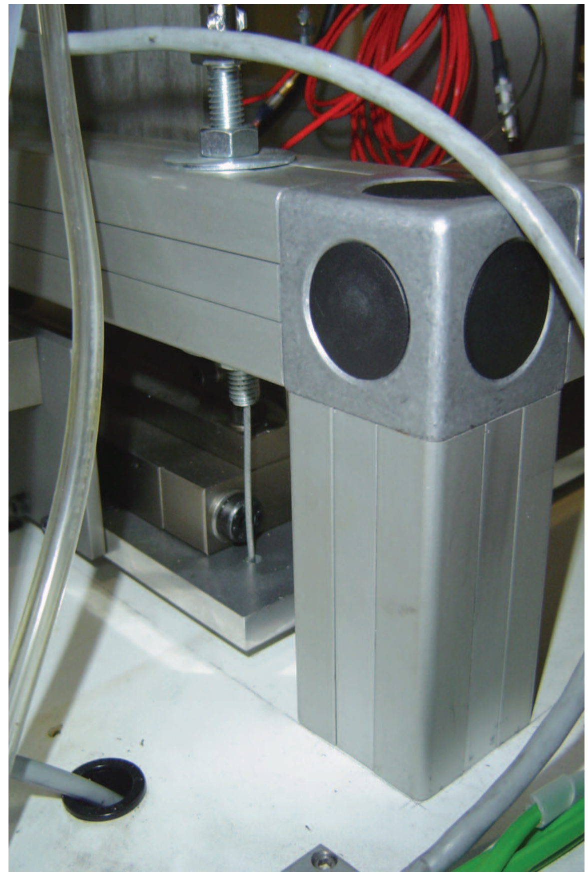

Fig. 3 Hanging plate supporting the engine and strapping system

These hardware modifications were all performed by students as part of their Master theses. They represent approximately 20 person-months of student work.

3.1 The Thrust Measurement. In its original configuration the jet engine was supported on two rigid "legs" and the thrust was actually a result of a correlation with the pressure in the combustion chamber.

To provide for free engine response to thrust, the support legs were removed and the engine was fixed on a rigid plate made of aluminum. This plate has also to support the (heavy) system used to actuate the variable area nozzle. The plate is free to react to the engine thrust as it hangs from the frame using four straps made from steel cables (Fig. 3). In order to improve the thrust response even further, all of the rigid tubing connections were replaced with flexible couplings (fuel and oil in and out, pressurized air in, and pressure and temperature measurements).

The load transducer is a commercially available standard load cell rated to 200 N (Sensy 2712). The sensitivity of this load cell is 1.85 mV/V. The load cell is mounted with two kneecaps to compensate for alignment errors. The jet engine is restrained axially by the load cell (Fig. 4). In order to calibrate the thrust measurement, a cable-pulley system was devised so that calibrated weights could be hung from the centerline of the jet engine. The system calibrated to a resolution of 0.2 N. The thrust measurement system also maintains zero and is repeatable.

3.2 The Airflow Measurement. The bell-mouth original nozzle (visible in Figs. 1 and 2) has been replaced with a calibrated nozzle (Fig. 5). The airflow is deduced from the difference between the ambient pressure and the static pressure measured by four holes at the throat of the flowmeter. The accuracy is 5 g/s.

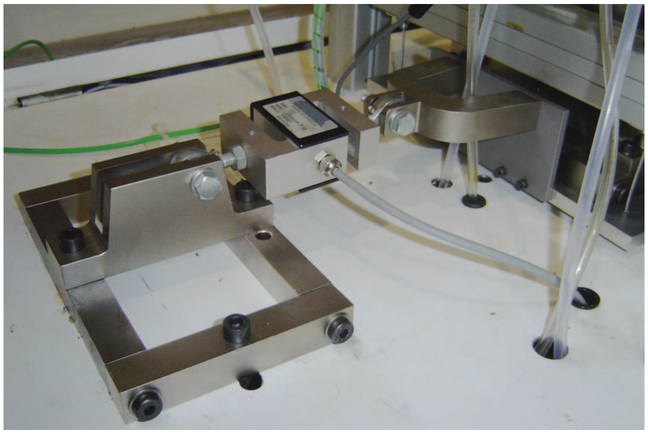

Fig. 4 Thrust measuring load cell

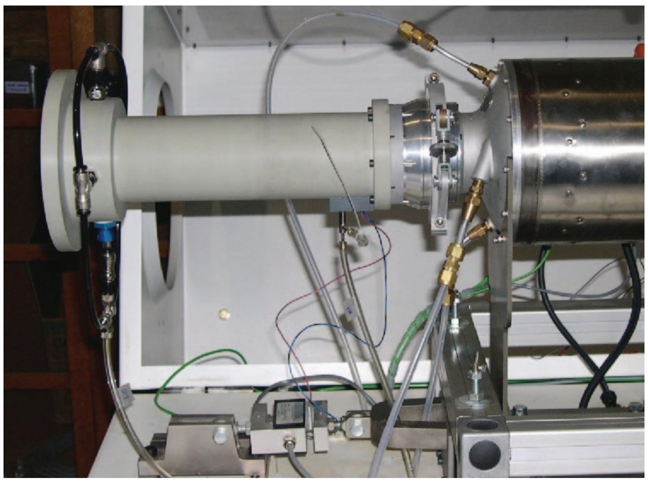

Fig. 5 Air flowmeter and variable geometry inlet guide vane

3.3 The Fuel Flow Measurement. The fuel flow is measured using a volumetric sensor similar to those used for diesel engines. The sensor consists of a cavity with a known reference volume that fills and empties according to the fuel flow sent to the injectors and to the fuel flow returning to the tank. A pulse is sent to an electronic device each time the cavity is filled up. The fuel flow is simply obtained by multiplying the frequency of this signal by the reference volume of the cavity. The accuracy is 0.5% of the full scale value.

3.4 The Variable Area Nozzle. The original engine is operated by controlling the fuel flow, which is injected into the combustion chamber. Varying the fuel flow allows traversing the equilibrium line of the engine from idle (around 40,000 rpm) to maximum speed (around 85,000 rpm). It was decided to add a second control parameter to the engine, in order to vary the position of the equilibrium line and to allow for the exploration of the compressor map. This has been done through the addition of a variable area convergent nozzle as a prolongation of the existing one. Figure 6 depicts a cut view of the SR-30 engine featured with the variable area nozzle.

The inlet section of the variable area nozzle is circular and fits the exit section of the original one. The outlet section is rectangular and has the same area as the inlet section ($2462\ \text{mm}^2$). The transition from the circular inlet to the rectangular outlet is progressive and based on a combination of conical and plane surfaces. Two movable flaps allow decreasing the outlet section down to 20% of the initial area (which is far beyond the limits of the engine in terms of EGT). Of course as the outlet section area can only decrease compared with the original value the engine running line can only be shifted upward. However, a nozzle with a wider outlet section would have acted as divergent-convergent for most of the operating conditions, with the related pressure drop. This solution was not selected considering the relatively low total pressure (around 1.3 bars) at the turbine outlet section. It is recognized that this extra nozzle did not allow a sufficient exploration of the compressor characteristic since the operating points with the minimum loss could not be reached.

The variable area nozzle is 170 mm long and is made of Inconel 625 using an electro-erosion machine. It is mounted on the engine using the six original screws that are used to fix the rear plate to the original nozzle liner. The rotation of the two flaps is performed

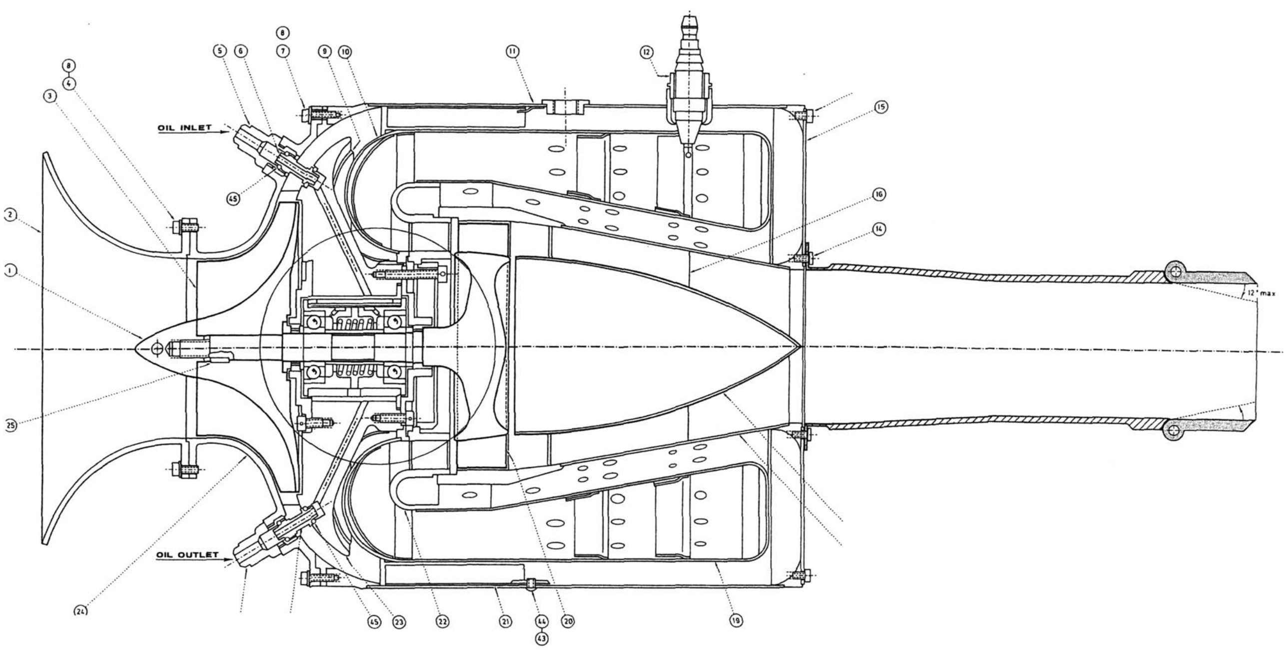

Fig. 6 The SR-30 and the variable area nozzle

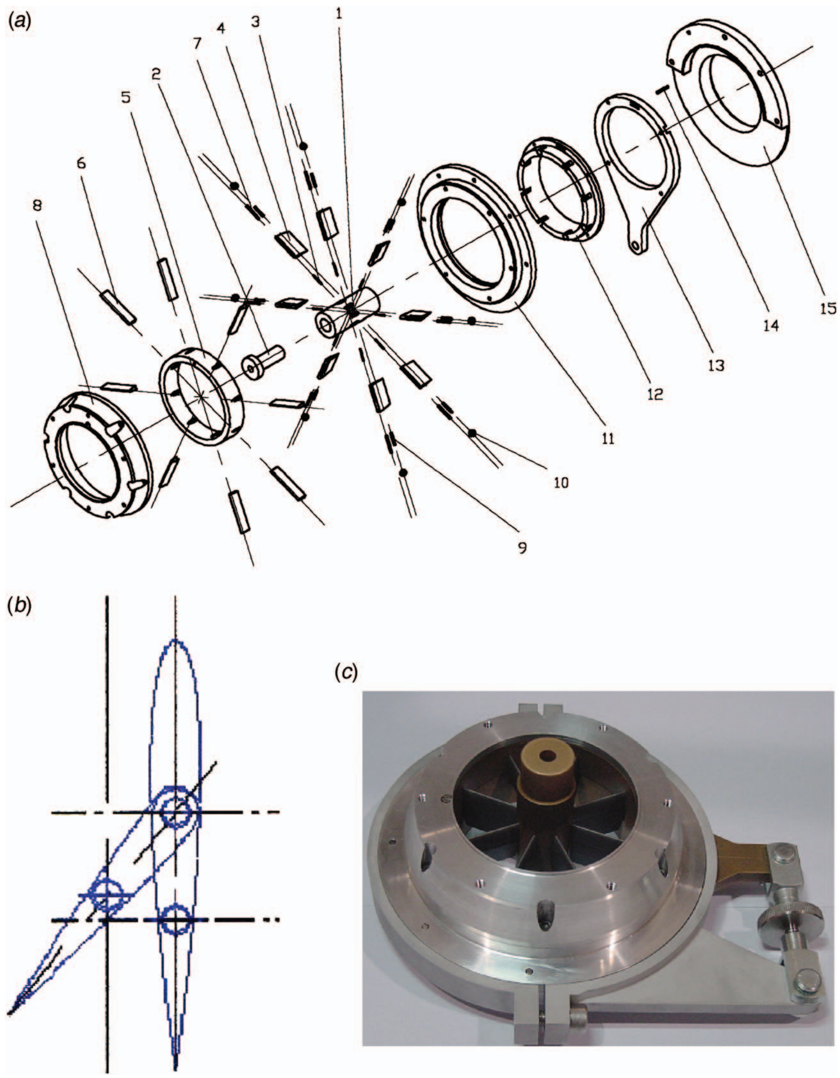

Fig. 7 Inlet guide vane

using a dc servomotor and a notched belt (visible in Fig. 8). It can be either operated manually or included in a control loop.

3.5 The Variable Geometry Inlet Guide Vane. With the same objective of controlling the operating point of the engine and widening its operational domain, it was decided to design and to build a variable geometry guide vane and to mount it between the original bell-mouth nozzle (or the flowmeter nozzle) and the inlet section of the compressor.

The inlet guide vane (IGV) system is made of eight blades that can be rotated by -40 deg to $+40$ deg around the radial direction. The flow entering the rotor is deflected either in the sense of rotation or in the opposite sense. According to the Euler equation, which relates the enthalpy rise to the angular momentum variation within the rotor, the characteristic map of the compressor is significantly modified by the rotation of the eight blades at the price of a (moderate) pressure drop. The rotation of the aft-part of the blades results from the circular movement of a ring operated by a radial arm (Fig. 7).

3.6 The Fuel Valve. The original engine was controlled purely manually, only by modifying the quantity of fuel injected into the combustion chamber. The fuel valve actually controls the quantity of fuel, which is allowed to return to the fuel tank. A fully open valve therefore corresponds to idle and a fully closed valve corresponds to maximum speed. The fuel flow ranges from 2 g/s to 5 g/s approximately.

The real-time acquisition system has a number of inputs but also two possible outputs that can pass 0/10 V signals. It was decided to take advantage of this feature to remotely operate the fuel valve, since it should open the way to a digital control of the engine via the acquisition system (described in Sec. 5).

To this end the mechanical control of the fuel valve (using a cable) was replaced with a dc servomotor controlled either by a PC or by an angular position sensor on the original throttle lever so that a manual control is still available. The dc motor is connected to the fuel valve via a reduction gear and a parallelogram mechanism (Fig. 8).

4 Modeling the SR-30 Engine

Turbine engines can be modeled at various levels of detail, ranging from simple algebraic relations to full 3D description of the gas path. Among this variety, aerothermodynamic models (also known as 0D models) are largely used throughout an engine program: for preliminary design and performance prediction, for the engine-airframe integration, as well as for the synthesis of the control laws, and for condition monitoring. As a direct application of the course of Propulsion Physics, a number of Master theses have been partly dedicated to the development of such a 0D

Fig. 8 Rear part of the engine and fuel valve operating system

model of the SR-30 turbojet, which has been subsequently used for control system design and performance diagnostics. Reported here is the setup of the latest model [5].

0D models allow the prediction of the overall performance of an engine such as net thrust and specific fuel consumption and the average thermodynamic state of the working fluid at intercomponent stations. As the name suggests, the resolution of such models lies at a component level. Modeling the engine cycle relies on the application of mass, momentum, and energy balances along the engine flow-path.

ECOSIMPRO [6] was selected as the platform for the development of the engine model. This general simulation tool is object-oriented and based on the concept of component to model a system. It allows focusing on the modeling task itself as it features a powerful equation solver as well as a graphical user interface (ECODIAGRAM) for building the model. Figure 9 depicts a schematic of the SR-30 model in ECODIAGRAM. The major components of the engine are the flowmeter (intake), the compressor, the burner, the turbine, and the convergent nozzle.

As a first step, a library of components is created in ECOSIMPRO. Each component can be seen as an operator whose purpose is to compute the thermodynamic state of the fluid (typically mass flow W, total temperature T^0, and pressure p^0) at the outlet of the module on the basis of the inlet conditions and some additional parameters. The modeling relies on the equations for mass, momentum, and energy balances and/or on empirical information derived from rig tests or computational fluid dynamics (CFD) calculations (e.g., compressor and turbine maps). A number of textbooks, see for instance Refs. [7,8], are dedicated to this task.

4.1 Thermodynamic Properties. The working fluids (air and combustion gases) are considered as semiperfect gases of variable specific heats. Accordingly, the constant-pressure specific heat C_p, the enthalpy h, and the entropy function Φ are defined as

$$C_p = C_p(T,\mathrm{FAR}) \tag{1}$$

$$h = h_{\mathrm{ref}} + \int_{T_{\mathrm{ref}}}^{T} C_p dT = h(T,\mathrm{FAR}) \tag{2}$$

$$\Phi = \Phi_{\mathrm{ref}} + \int_{T_{\mathrm{ref}}}^{T} \frac{C_p}{T} dT = \Phi(T,\mathrm{FAR}) \tag{3}$$

where FAR is the fuel-to-air ratio.

4.2 Atmospheric Conditions and Flowmeter. The engine is mounted on a test bench. In that configuration, ambient pressure and temperature are also the total conditions at the flowmeter inlet (Station 1). The effect of humidity is not taken into account in the present model.

$$p_1^0 = p_{\mathrm{amb}} \tag{4}$$

$$T_1^0 = T_{\mathrm{amb}} \tag{5}$$

The flowmeter is supposed adiabatic, but introduces a pressure drop measured by a total pressure recovery factor π_d. The thermodynamic state of the fluid at the flowmeter exit (Station 2) is

$$W_2 = W_1 \tag{6}$$

$$T_2^0 = T_1^0 \tag{7}$$

$$p_2^0 = \pi_d\, p_1^0 \tag{8}$$

where π_d is given by the ISA-1932 norm that was followed to build the flowmeter.

4.3 Compressor. This component actually stacks the inlet guide vane and the centrifugal stage. The governing equations for the compressor are the following:

$$W_3 = W_2 \tag{9}$$

$$p_3^0 = \pi_c\, p_2^0 \tag{10}$$

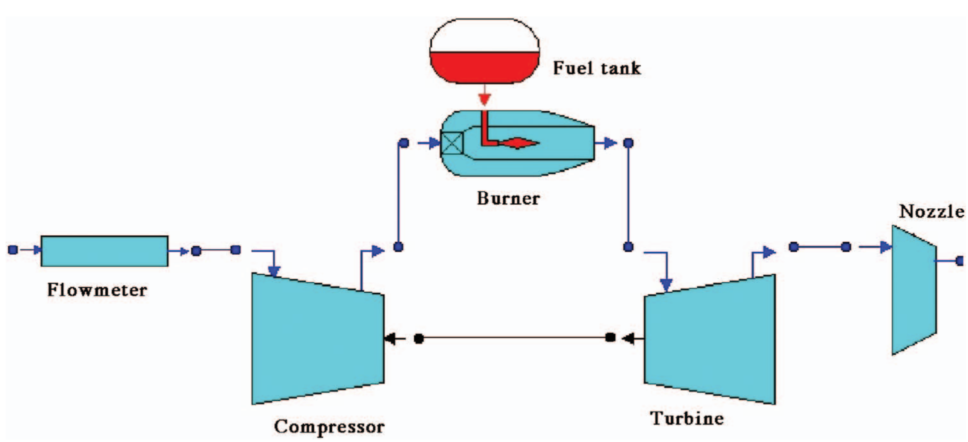

Fig. 9 Schematic of the ECOSIMPRO model

$$h_3^0 = h_2^0 + \frac{1}{\eta_c}(h_{3,\mathrm{is}}^0 - h_2^0) \quad (11)$$

The isentropic outlet enthalpy $h_{3,\mathrm{is}}^0$ is computed from the entropy function

$$\Phi_{3,\mathrm{is}} = \Phi_2 + R\,\log(\pi_c) \quad (12)$$

The characteristic curves of the compressor have been worked out from a mean-line analysis [9] and are stored in the β-lines format to prevent numerical interpolation problems. Accounting for the effect of the inlet guide vane, the corrected inlet mass flow W_2^{std}, the pressure ratio π_c, and the isentropic efficiency η_c are functions of the corrected spool speed N_2^{std}, the β-coordinate, and the IGV stagger angle α_{IGV} as follows:

$$W_2^{\mathrm{std}} = C_{W^{\mathrm{std}}}\, f_{W^{\mathrm{std}}}(N_2^{\mathrm{std}}, \beta, \alpha_{\mathrm{IGV}}) \quad (13)$$

$$\pi_c = C_\pi\, f_\pi(N_2^{\mathrm{std}}, \beta, \alpha_{\mathrm{IGV}}) \quad (14)$$

$$\eta_c = C_\eta\, f_\eta(N_2^{\mathrm{std}}, \beta, \alpha_{\mathrm{IGV}}) \quad (15)$$

where $C_{W^{\mathrm{std}}}$, C_π, and C_η are so-called map scaling factors that are applied to the performances read in the map so that they match the actual compressor performances.

The power required to drive the compressor is given by

$$\mathrm{PW}_c = W_3(h_3^0 - h_2^0) \quad (16)$$

4.4 Burner. The combustion chamber increases the enthalpy of the working fluid through the burning of fuel. The governing equations for this component are

$$W_4 = W_3 + W_F \quad (17)$$

$$p_4^0 = \pi_b\, p_3^0 \quad (18)$$

$$h_4^0 = \frac{\eta_b W_F \mathrm{LHV} + W_3 h_3^0}{W_4} \quad (19)$$

where LHV stands for low heating value of the fuel.

The combustion efficiency η_b expresses the fact that the combustion process is incomplete. It is very well correlated with the air loading AL as follows:

$$\mathrm{AL} = \frac{W_3}{\mathrm{vol}(p_3^0)^{1.8} 10^{0.00145(T_3^0 - 400)}} \quad (20)$$

The pressure recovery factor π_b accounts for the friction losses and is evaluated according to

$$\pi_b = 1 - K_b\left(\frac{W_3\sqrt{T_3^0}}{p_3^0}\right)^2 \quad (21)$$

where K_b is a constant depending on the burner geometry and surface roughness.

4.5 Turbine. The constitutive equations for the turbine are quite similar to those of the compressor as follows:

$$W_5 = W_4 \quad (22)$$

$$p_5^0 = \pi_t\, p_4^0 \quad (23)$$

$$h_5^0 = h_4^0 + \eta_t(h_{5,\mathrm{is}}^0 - h_4^0) \quad (24)$$

The isentropic outlet enthalpy $h_{5,\mathrm{is}}^0$ is computed from the entropy function

$$\Phi_{5,\mathrm{is}} = \Phi_4 + R\,\log(\pi_t) \quad (25)$$

Due to the moderate compressor pressure ratio, the turbine is unchoked for most of the operating regimes. Moreover, no map is available, be it from the manufacturer or from a mean-line analysis. As a workaround, Stodola's ellipsis is used for describing the pressure ratio π_t-corrected mass flow W_4^{std} relation

$$W_4^{\mathrm{std}} = K_t\sqrt{1 - \pi_t^{n_t}} \quad (26)$$

where K_t and n_t are constant parameters that characterize the turbine stage. Stodola's model treats the turbine as a nozzle, as far as the $(W_4^{\mathrm{std}}, \pi_t)$ curve is concerned, and therefore neglects the influence of the rotational speed on the stage characteristic.

Considering the isentropic efficiency η_t, a correlation with the inlet corrected mass flow is to be determined from the experimental measurements.

The available power generated by the turbine is given by

$$\mathrm{PW}_t = \eta_m W_4(h_4^0 - h_5^0) \quad (27)$$

The mechanical efficiency η_m accounts for the loss generated in the bearings supporting the shaft.

4.6 Exhaust Nozzle. Assuming an adiabatic process, the constitutive equations write down

$$W_9 = W_5 \quad (28)$$

$$p_9^0 = \pi_n p_5^0 \quad (29)$$

$$T_9^0 = T_5^0 \quad (30)$$

where π_n represents the pressure loss across the nozzle and is modeled as the burner pressure loss (21).

The nozzle expansion ratio $\mathrm{NER} = p_{\mathrm{amb}}/p_9^0$ is subcritical for the whole operating range, which means that the static pressure in the exit plane p_9 is equal to the ambient pressure p_{amb} and the exhaust Mach number is subsonic. From the exit Mach number M_9 and total temperature T_9^0, the exhaust jet velocity V_9 can be computed with usual equations. A discharge coefficient C_D is introduced to account for the reduction of effective flow area due to the boundary layer. C_D is correlated with the NER as follows:

$$C_D = \frac{A_{9,\mathrm{eff}}}{A_{9,\mathrm{geom}}} = C_D(\mathrm{NER}) \quad (31)$$

Finally, the thrust generated by the engine is assessed with a momentum balance between the engine inlet and outlet as follows:

$$FG = W_9 V_9 + A_{9,\mathrm{eff}}(p_9 - p_{\mathrm{amb}}) \quad (32)$$

The net thrust confounds with the gross thrust since the engine is not moving and the pressure term vanishes as the nozzle is unchoked.

4.7 Assembling the Components. To build the engine model, the basic modules presented in Secs. 4.1 through 4.6 are assembled following the general schematic of Fig. 9. Ensuring the conservation of mass, momentum, and energy throughout the engine generates constraints, which actually restrict the operating range of each component. The conservation principles translate into a set of nonlinear algebraic equations, also termed compatibility equations that are solved with ECOSIMPRO's built-in algorithms.

From an external point of view, the engine model can be seen as a vector-valued function

$$y = \mathcal{G}(u) \quad (33)$$

where u is the vector of command parameters that define the operating point of the engine (fuel flow, nozzle area, IGV angle, ambient temperature, and pressure) and y is the vector of measurements (total temperature and pressure at various stations, spool speed, and thrust).

4.8 Fitting the Engine Model to Test Data. Numerous parameters have appeared in the modeling of the components. Their values must be determined on the basis of experimental data collected on the engine so that the resulting model is representative of the actual engine behavior. This task is usually known as model

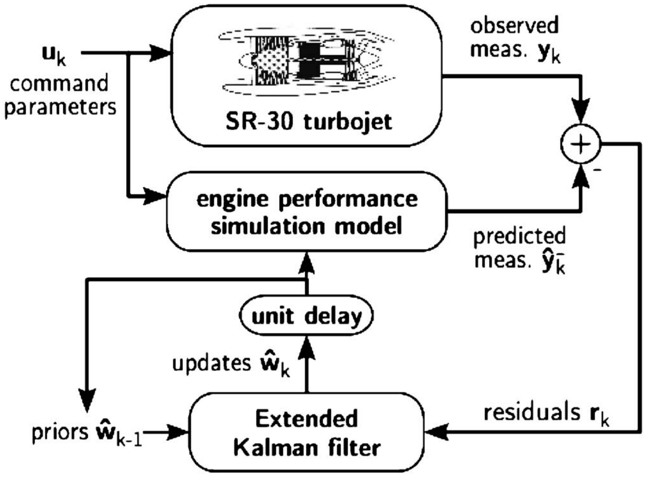

Fig. 10 Tuning procedure using an extended Kalman filter

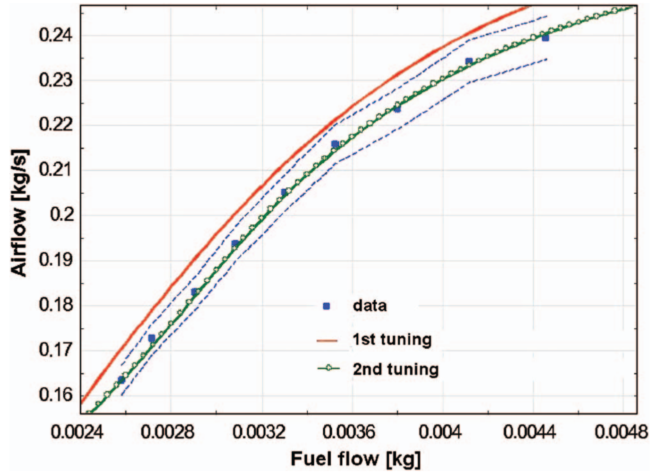

Fig. 12 Fuel flow—airflow curve

fitting/tuning. Data have been collected on the engine in the operating range 55,000–75,000 rpm per steps of 2500 rpm. The tests were conducted at a nominal IGV stagger and a fully opened nozzle.

Model fitting has been carried out in two stages. Raw estimations of the various parameters and correlations have been determined from a first tuning procedure applied to each component separately. As some important quantities are not available (e.g., turbine inlet total pressure p_4^0) or are at best rough indicators (e.g., turbine inlet total temperature T_4^0), the values of some parameters such as mechanical efficiency or burner pressure loss have been imposed to common values.

Second, a fine tuning of the model has been performed. The fitting parameters are now computed at a global level. To this end, they are considered as additional inputs w of the model:

$$y = \mathcal{G}(u,w) \tag{34}$$

The tuning task can be seen as the inverse problem of performance prediction. Knowing the command parameters u and the observed measurements y, the parameters w are modified so that the residuals between the experimental data and the model predictions are minimized in the least-squares sense. The minimization algorithm implements a Kalman filter (see Ref. [10] for details) developed in the Turbomachinery Group in the frame of research activities in health monitoring. Figure 10 sketches the general principle of the recursive tuning of model parameters.

Some results of the fitting procedure are sketched in Figs. 11 and 12. The blue dots are the experimental data, the dotted blue lines are the uncertainty bounds on the measurements, the red line is the model prediction after the first tuning step, and the green line is the model prediction after refining the parameter values with the Kalman filter.

Figure 11 depicts the evolution of the exhaust gas temperature T_9^0 with respect to the fuel flow. It can be seen that the model predictions are already within the uncertainty bounds for the higher operating regimes after the first tuning process. The second pass with the Kalman filter improves the results in the mid- and low-power regions.

Figure 12 represents the evolution of the airflow W_2 with respect to the fuel flow. For this particular quantity, the first tuning procedure is clearly unsuccessful as the prediction of airflow is outside the confidence limits for the whole operating line. The further fitting performed by the Kalman filter dramatically improves the quality of the mass flow prediction for the regimes considered. Conclusions similar to those drawn for Figs. 11 and 12 are valid for the other measurements.

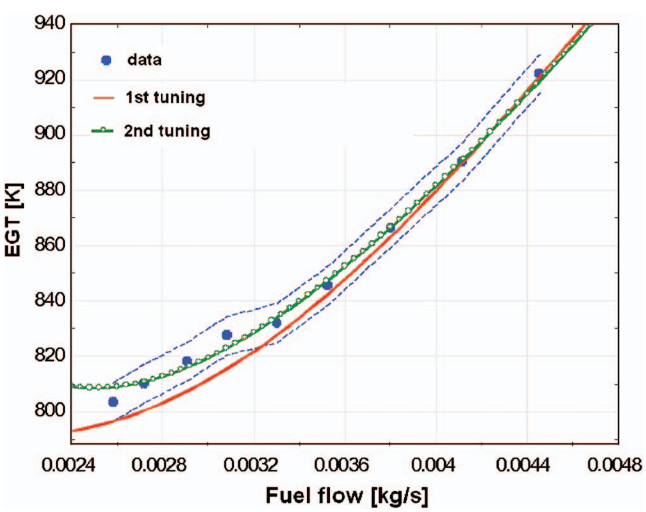

Fig. 11 Fuel flow—EGT curve

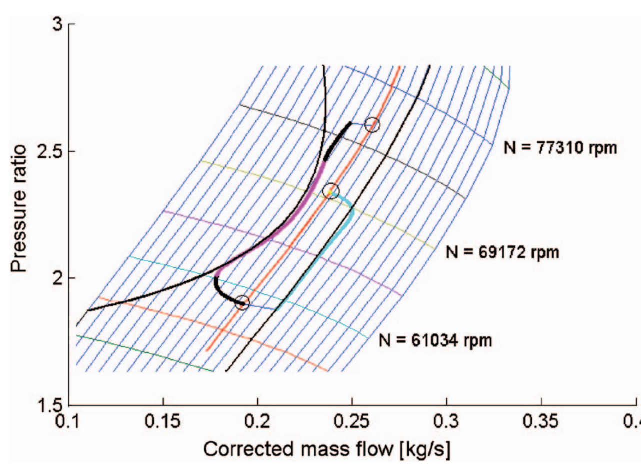

Fig. 13 Trajectory of the operating point for a deceleration followed by an acceleration in the compressor map: steady-line (red curve), limits on the mass flow (black curves), and steady operating points (black circles)

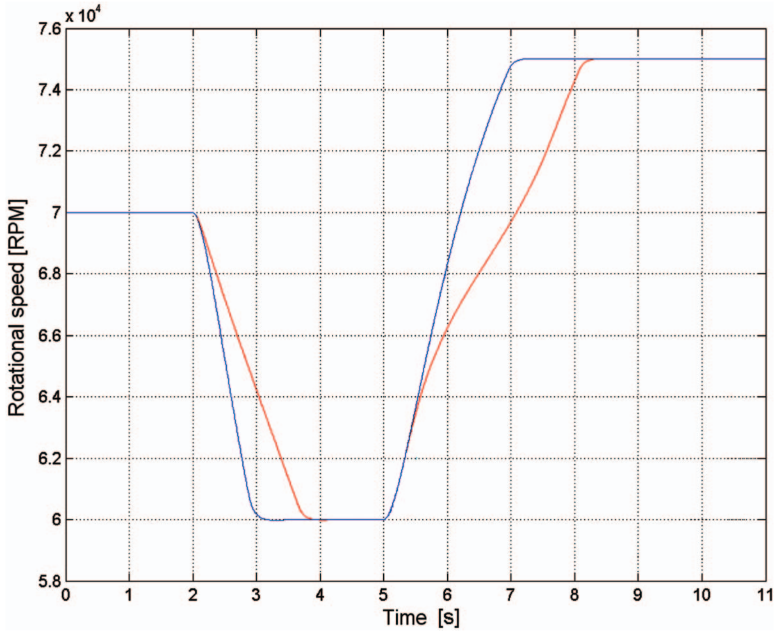

Fig. 14 Evolution of the rotational speed with (red line) and without (blue line) physical limits

5 Controlling the SR-30 Engine

A transient mathematical model of the engine can be made available by adding one equation to the steady-state model described above. This equation describes the evolution of the rotational speed with time by balancing the power developed by the turbine, the power required by the compressor, and the inertia of the rotating parts as follows:

$$J\left(\frac{2\pi}{60}\right)^2 N\frac{dN}{dt} = \mathrm{PW}_t - \mathrm{PW}_c \qquad (35)$$

Whereas the dynamic behavior of the rotational speed is captured with some accuracy provided that the additional parameter J in Eq. (35) is correctly determined, the evolutions of the mass flow and the temperatures are more qualitatively captured. As the acquisition system is able to output signals and as the fuel valve is driven now by a dc motor, it was decided to explore the possibility of controlling the fuel flow injected into the engine corresponding to prescribed objectives.

The objectives are the minimization (at least the reduction) of the time required for transients, while avoiding the trespass of any physical limit of the engine. The rotational speed has been selected to play the role of the performance parameter from which a feedback action is determined, as it is the case on most of gas turbine engines. The physical limits are specified in terms of rotational speed (minimum and maximum levels), air and fuel flows (minimum and maximum values), and maximum EGT.

A controller has been devised for this virtual engine using MATLAB/SIMULINK. The control device includes the following elements: a feedforward action that generates a command, a feedback action that generates a correction of the feedforward in function of the error, one control action per physical limit, and an antiwindup device. The control strategy has to pursue the following objectives: reduction of the response time, zero static error, no violation of any of the physical limits, robustness against external perturbations, and sensor noise. A proportional-integral-derivative control law has been selected for the rotational speed (tuned with the performance index ITAE[1]), while a proportional-integral control law was selected for the air mass flow as well as for the EGT (for a very short response time).

An example of control sequence is depicted in Fig. 13. The engine decelerates from 70,000 rpm to 60,000 rpm, and stabilizes and accelerates up to 75,000 rpm. The operating point moves between the following physical limits: minimum fuel flow (yellow), maximum corrected mass flow (cyan), maximum fuel flow (black), minimum corrected mass flow (magenta), and maximum fuel flow again.

The corresponding evolution of the rotational speed is depicted in Fig. 14 (red curve). The latter is compared with the speed obtained in the absence of limits (blue curve). While the setting time is of the order of 10 s for the open-loop engine, it has been reduced to about 1 and 2 s for the unlimited maneuvers depicted here. Even in the case of limits, the closed-loop behavior remains very rapid. For several reasons these results obtained with the ECOSIMPRO transient mathematical model coupled to a MATLAB/SIMULINK controller could not be repeated on the test bench.

The dynamic behavior of the fuel valve actuation is characterized by a considerable inertia due to the parallelogram system (visible in Fig. 8). This means that if the dynamics of the closed loop is too rapid the inertia of the fuel valve is stronger than the damping, resulting in a violation of physical limits. This issue has shown to significantly limit the performance of the controller. The performance of the controller is even more limited by the acquisition frequency of 4 Hz and its associated time delay of 250 ms between the computation of the command signal and the moment at which the latter is applied.

For these reasons the control laws synthesized and tested with the mathematical model of the engine had to be significantly modified with a loss of performance. The bandwidth of the controller had to be drastically limited, i.e., the closed-loop behavior of the engine had to be smoothed to avoid instabilities.

Figure 15 illustrates the poor performance of the fuel controller facing an external perturbation introduced by a rapid opening of the variable area nozzle. The ejection velocity is reduced and so is the total pressure in the nozzle, inducing an acceleration of the engine spool. The rejection of this perturbation, while effective, is slow and oscillating.

The high frequency/small amplitude evolutions observed in Fig.

[1]Integral of time multiplied by absolute error: ITAE$=\int_0^T t|e(t)|dt$.

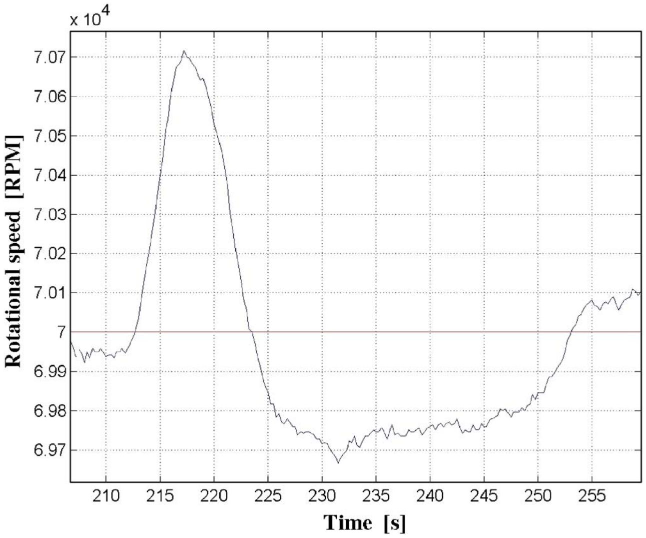

Fig. 15 Rejection of an external perturbation

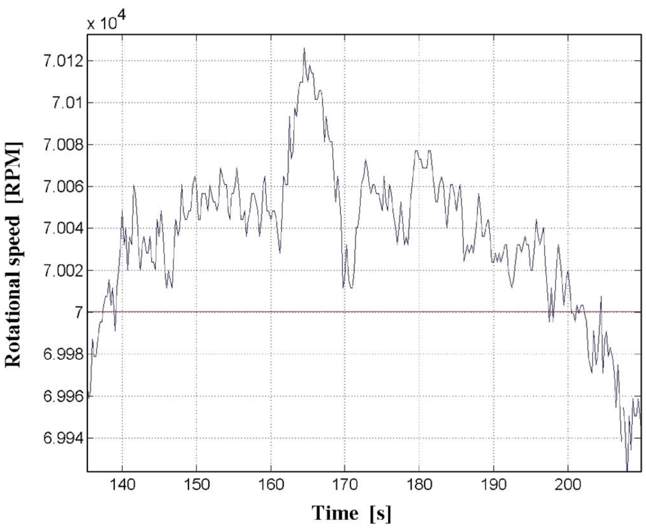

Fig. 16 Follow-up of a prescribed rotational speed

15 (and further in Fig. 16) are probably the consequence of additional poor features of the fuel valve actuator. The latter introduces strong nonlinearities due to internal friction forces, inducing parasitic movements of the fuel valve and degrading the transient performance of the whole system. The command noise characterizing the original fuel valve actuation is another issue. It is due to the necessary clearance in the kneecap mechanisms of the parallelogram system.

Figure 16 illustrates the result of the follow-up of an assigned value for the rotational speed equal to 70,000 rpm. The maximum error is about 100 rpm, but the mean error is below 50 rpm, which can be considered as rather successful considering the above mentioned shortcomings of the actuation system.

The replacement of the original fuel valve and its actuation system with a proportional electrical valve whose dynamics is fast enough seems to be the only way to overcome these problems. This solution has been implemented by Watanabe et al. [1] and has been undertaken this year in our group by a Master student.

6 Conclusions

The main characteristic of gas turbines, i.e., power density, is well illustrated by the SR-30 engine, which is a reliable and effective demonstrator of many aspects of gas turbine operation. As noted by other academic teams, the single-point one-dimensional instrumentation typical of this small scale engine makes it somewhat difficult to obtain accurate results. However, the SR-30 is an excellent opportunity for the students to learn about the limitations of simplifying assumptions and about the difficulty associated with data acquisition, treatment, and interpretation.

The development of a computer model of the engine has shown that, by coupling principles of thermodynamics and mechanics to measured data and to a smart parameter identification procedure, it is possible to obtain meaningful results, despite the lack of information about component performance (no compressor nor turbine maps are available). These results would not have been obtained without the additional instrumentation, i.e., airflow, fuel flow, or thrust measuring devices.

The modifications of the test bench to implement these additional sensors, the design, the development, and the implementation of additional components for the engine itself, such as an inlet guide vane or a variable area nozzle, as well as the tentative to control the engine via the acquisition system, represented very appealing projects for the students. These projects were also quite successful in terms of educational objectives because they implied a deep understanding of the physics of many phenomena.

Acknowledgment

This work has been performed by the following Master students: Pierre-Yves Hanquet (thrust measurement), Anthony Mignon (variable area nozzle), Pierre Seronveaux (actuation via dc motors), Benoît Vertessen (design of the inlet guide vane), Claude Mockels (integration of the inlet guide vane), Jean-Philippe Thomas (new thrust measurement frame and control of the engine), Khanh Mai Quoc (identification of the engine model), and François Denis (proportional electrical fuel valve). The success of the SR-30 in our laboratory is also due to the strong support of its manufacturer, despite the distance.

Nomenclature

A = area
FG = thrust
h, h^0 = enthalpy, total enthalpy
J = spool inertia
N = spool speed
p, p^0 = pressure, total pressure
PW = power
R = gas constant
T, T^0 = temperature, total temperature
W, W_F = air mass flow, fuel mass flow
η = isentropic efficiency
Φ = entropy function
π = pressure ratio

Subscripts and Superscripts

1 = intake inlet
2,3 = compressor inlet, compressor outlet
4,5 = turbine inlet, turbine outlet
9 = exhaust
b = burner
c = compressor
t = turbine
amb = ambient
is = isentropic
std = corrected for standard conditions

References

[1] Watanabe, A., lmen, S. M., Leland, R., Whitaker, K. W., and Trevino, L. C., 2004, "Soft Computing Applications on SR-30 Turbojet Engine," AIAA Paper No. 2004–6444.
[2] Perez-Blanco, H., 2003, "Activities Around the SR-30 Minilab at PSU," *Proceedings of the 2003 American Society for Engineering Education Annual*

Conference and Exposition, The American Society for Engineering Education, Nashville, TN.
[3] Witkowski, T., White, S., Ortiz Dueas, C., Strykowski, P., and Simon, T., 2003, "Characterizing the Performance of the SR-30 Turbojet Engine," *Proceedings of the 2003 American Society for Engineering Education Annual Conference and Exposition*, The American Society for Engineering Education, Nashville, TN.
[4] Turbine Technologies Ltd, http://www.turbinetechnologies.com
[5] Mai, Q.-K., 2006, "Simulation of the Performance of the SR-30 Turbojet (in French)," M.S. thesis, University of Liège, Liège, Belgium.
[6] EcosimPro by EA Internacional, http://www.ecosimpro.com
[7] Mattingly, J. D., 1996, *Elements of Gas Turbine Propulsion*, McGraw-Hill, Singapore.
[8] Walsh, P. P., and Fletcher, P., 1998, *Gas Turbine Performance*, Blackwell Science, Oxford.
[9] Vertessen, B., 2001, "Design of a Variable Guide Vane for the SR-30 Turbojet (in French)," M.S. thesis, University of Liège, Liège, Belgium.
[10] Dewallef, P., 2005, "Application of the Kalman Filter to Health Monitoring of Gas Turbine Engines: A Sequential Approach to Robust Diagnosis," Ph.D. thesis, University of Liège, Liège, Belgium.